Rare Met. (2023) 42(4):1403–1407
https://doi.org/10.1007/s12598-017-0993-7

RARE METALS
www.editorialmanager.com/rmet

Coercivity enhancement of hot-deformed Nd–Fe–B magnets with Pr–Cu alloy addition

Jun-Ming Wang, Zhao-Hui Guo*, Zheng Jing, Xiao Du, Neng-Jun Yu, Meng-Yu Li, Ming-Gang Zhu, Wei Li

Received: 11 October 2016 / Revised: 18 January 2017 / Accepted: 25 November 2017 / Published online: 5 January 2018

Abstract Effects of low-melting Pr–Cu alloy addition on the microstructure and magnetic properties of the hot-deformation Nd–Fe–B magnets were investigated. A small amount of Pr–Cu addition enhances the coercivity of the hot-deformation Nd–Fe–B magnets obviously. The coercivity of the hot-deformation Nd–Fe–B magnets with 4.0 wt% $Pr_{85}Cu_{15}$ addition increases to 1271 kA·m^{-1}, 75.69% higher than that of Pr–Cu-free magnet (723 kA·m^{-1}), and then decreases with 5 wt% $Pr_{85}Cu_{15}$ addition. It is observed that there a uniform RE-rich phase is formed wrapping the $Nd_2Fe_{14}B$ main phase in the sample with 4.0% $Pr_{85}Cu_{15}$ addition by scanning electron microscopy (SEM), which promotes the coercivity. The angular dependence of coercivity for the hot-deformation Nd–Fe–B magnets indicates that the coercivity mechanism is nucleation combined with domain wall pinning. The domain wall pinning is weakened, while the nucleation is enhanced after Pr–Cu addition. The remanence, intrinsic coercivity, and maximum magnetic energy product of the original Nd–Fe–B magnet are 1.45 T, 723 kA·m^{-1}, and 419.8 kJ·m^{-3}, respectively, and those of the sample with 4.0% $Pr_{85}Cu_{15}$ alloy addition are 1.30 T, 1271 kA·m^{-1}, and 330.0 kJ·m^{-3}, respectively.

Keywords Nd–Fe–B; Low-melting alloy; Hot-deformation; Microstructure; Coercivity mechanism

J.-M. Wang, Z.-H. Guo*, Z. Jing, X. Du, N.-J. Yu, M.-Y. Li, M.-G. Zhu, W. Li
Division of Functional Materials, Central Iron & Steel Research Institute, Beijing 100081, China
e-mail: zhguo@vip.sina.com

1 Introduction

Hot-deformation process has drawn much attention due to its advantages on obtaining high corrosion resistance, good magnetic properties, and complicated shape anisotropic Nd–Fe–B magnets [1–3]. The platelet-like grains were surrounded by thin Nd-rich intergranular phase [4], and the average grain size of the hot-deformation Nd–Fe–B magnets is typically ~ 100 nm in thickness and 300–800 nm in width [5, 6]. A strong (00*l*) texture develops during the hot-deformation or upsetting process [7, 8], which is considered to be due to the orientation dependent grain growth of tetragonal Nd_2Fe14_B phase [9–12] or the anisotropy of its elastic properties [13]. The ultrafine grain size of the hot-deformation magnets is nearly a single domain size [14, 15], which indicates that the hot-deformation magnets have potential for achieving higher coercivity [16, 17] compared with the sintered Nd–Fe–B magnets with several micrometers in grain size. Low-melting eutectic grain boundary diffusion process was found to be capable of improving coercivity for the hot-deformation magnets [18–20]. However, the diffusion process only works in a very limited depth which is hard to meet the production requirements. Another practical method to increase the coercivity is substituting heavy rare earth elements such as Dy and Tb for Nd. This is because that Dy-substituted phase has a higher magnetocrystalline anisotropy than the Nd–Fe–B phase [21, 22]. Hot-pressing the mixed powders of melt-spun Nd–Fe–B ribbons with DyF_3 and DyCu alloy and subsequent hot-deformation were found to be effective for improving coercivity [23–25]. Whereas Dy is a limited natural resource, securing a constant supply of Dy for enhancing Nd–Fe–B coercivity is not a sustainable way. It was reported that the low coercivity was due to the long-range magnetostatic interaction between $Nd_2Fe_{14}B$ grains

through a ferromagnetic intergranular phase that contains a high concentration of Fe or Co. It is revealed that a suitable Nd–Cu alloy addition will enhance coercivity of the hot-deformed magnets [26]. Thus, refining the grain boundary phase is an effective way to improve coercivity.

High coercivity Dy-free anisotropic nanocrystalline hot-deformed Nd–Fe–B magnets by Pr–Cu alloy addition were prepared in this paper. The microstructure was observed by a backscattered electron scanning electron microscopy (BSE-SEM) in order to obtain guideline to enhance the coercivity furtherly. The coercivity mechanism was investigated by angular dependence of coercivity.

2 Experimental

$Pr_{85}Cu_{15}$ (wt%) eutectics with optimized crystalline ribbons have been obtained by arc-melt and subsequently melt-spun at a wheel speed of 25 $m{\cdot}s^{-1}$. The $Pr_{85}Cu_{15}$ powders were sieved with a mesh size of 200 μm and mixed with Dy-free MQU-C melt-spun ribbons (Molycorp Magnequench) with composition of $Nd_{12.6}Fe_{77.1}Ga_{0.42}Co_{4.4}B_{5.5}$ (at%). The mixed powders were hot-pressed at 550 °C and subsequent hot-deformed at 840 °C. The magnetic properties of the samples with different $Pr_{85}Cu_{15}$ alloy additions were measured by a NIM-2000H hysteresisgraph. The crystal alignment was studied by using X-ray diffractometer (XRD, X'pert Pro) with Cu Kα radiation. BSE-SEM observations were made on the bulk samples using a field emission scanning electron microscope (JSM-7001F) at an acceleration voltage of 15.0 kV. The angular dependence of coercivity was measured by a vibrating sample magnetometer (VSM, VersaLab) with the maximum field of 2.3 $mA{\cdot}m^{-1}$ at room temperature.

3 Results and discussion

Figures 1 and 2 show the demagnetization curves of the hot-deformation Nd–Fe–B magnets with different $Pr_{85}Cu_{15}$ additions. The remanence (B_r) and maximum magnetic energy product [$(BH)_{max}$] decrease with the increase in alloy addition, which are mainly caused by the decrease in 2:14:1 Nd–Fe–B main phase ratio. The intrinsic coercivity (H_{cj}), B_r and $(BH)_{max}$ of the Nd–Fe–B magnet without and with 4.0 wt% $Pr_{85}Cu_{15}$ are, respectively, 723 $kA{\cdot}m^{-1}$, 1.45 T, 419.8 $kJ{\cdot}m^{-3}$, and 1271 $kA{\cdot}m^{-1}$, 1.30 T, 330.0 $kJ{\cdot}m^{-3}$. The coercivity reaches the highest value of 1271 $kA{\cdot}m^{-1}$ when the $Pr_{85}Cu_{15}$ addition is 4.0 wt%. It enhances by 75.69% compared with that of the original Nd–Fe–B magnets without $Pr_{85}Cu_{15}$ alloy, showing a tendency of increase and then decrease.

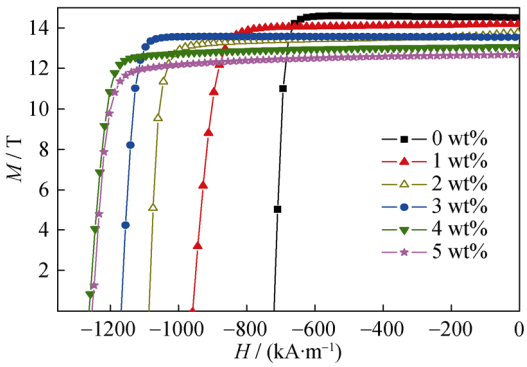

Fig. 1 Demagnetization curves of magnets with different $Pr_{85}Cu_{15}$ additions

XRD patterns of the hot-deformed samples with different $Pr_{85}Cu_{15}$ alloy additions are shown in Fig. 3. The patterns were obtained from the plane perpendicular to the pressure direction for all the samples. According to XRD patterns, the strong intensity of the (105) and (006) characteristic peaks of 2:14:1 phase indicates obvious texture formed in hot-deformed magnets. Although intensity ratio $R = I(006)/I(105)$ decreases after $Pr_{85}Cu_{15}$ alloy addition, the magnets still present a good texture orientation.

Figure 4a, c, e shows BSE-SEM images of the hot-deformed samples with 0 wt%, 4 wt%, 5 wt% Pr–Cu alloy additions. The patterns were taken from the plane

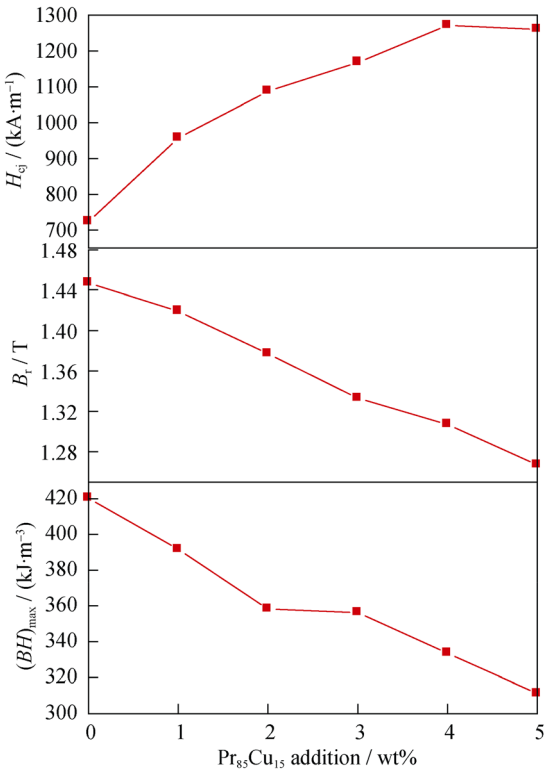

Fig. 2 Magnetic properties of magnets with different $Pr_{85}Cu_{15}$ additions

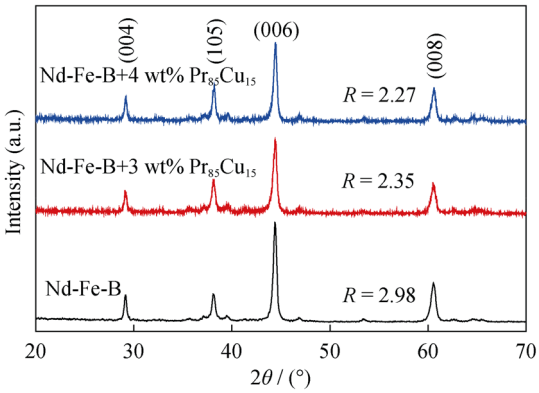

Fig. 3 XRD patterns of hot-deformed magnets with different $Pr_{85}Cu_{15}$ additions ($R = I(006)/I(105)$)

perpendicular to the *c*-axis. The *c*-axis is parallel to pressure direction and is out-plane, as the arrow indicates. The dark gray regions are $Nd_2Fe_{14}B$ phase, while the bright regions correspond to the RE-rich phase according to the energy spectrum analysis. The RE-rich phase distribution around the $Nd_2Fe_{14}B$ main phase is scattered in Pr–Cu-free sample (Fig. 4a). The content of RE-rich phase of the sample with Pr–Cu addition increases, and this phase is distributed uniformly around the $Nd_2Fe_{14}B$ phase, as shown in Fig. 4c. When Pr–Cu alloy increases to 5 wt%, the RE-rich layer becomes thicker than that with 4 wt% addition and there appear some large bright regions unevenly distributed. The result indicates that a suitable Pr–Cu alloy addition leads to more RE-rich around the main phase and uniform distribution. The neighboring grains are separated by a suitable RE-rich layer which weakens the long-range magnetostatic interaction of neighboring grains. According to the following equation [20],

$$H_c(T) = \alpha H_A(T) - N_{eff} M_s(T) \quad (1)$$

where α is the structure factor, $H_A(T)$ is the anisotropy field, N_{eff} is the effective demagnetization factor, and $M_s(T)$ is the saturation magnetic polarization; the value of N_{eff} decreases because the range magnetostatic interaction is weakened after Pr–Cu addition, resulting in the coercivity enhancement.

Figure 4b, d, f shows BSE-SEM images of the hot-deformed samples with 0 wt%, 4 wt%, 5 wt% Pr–Cu alloy additions taken from the plane which parallels to *c*-axis. The images show that the RE-rich phase layer [27] becomes thicker with the increase in Pr–Cu addition. There are some large bright areas unevenly distributed, and the RE-rich layer is so thick that it can hardly be separated when 5 wt% Pr–Cu alloy was added in the magnet.

Figure 5a, b shows angular dependence of half-hysteresis loops of the hot-deformed magnets, and θ means the angle between the external applied field and the magnetic aligned axis of the magnets. The angular dependence of coercivity (H_c) for the hot-deformation magnets, Stoner–Wohlfarth domain wall pinning model [28], and nucleation mechanism model developed by Kronmüller [29] is shown in Fig. 5c. The $H_c(\theta)/H_c(0)$ decreases firstly, then increases with θ changing from 0° to 75°, and reaches the maximum at 75° as shown in Fig. 5c. When θ changes from 0° to 75°, the curve changes nearly at a constant slope with the decrease of H_c, and the curve slope becomes larger and larger with the increase of H_c. The tendency of H_c means that the coercivity mechanism of the hot-deformed magnets

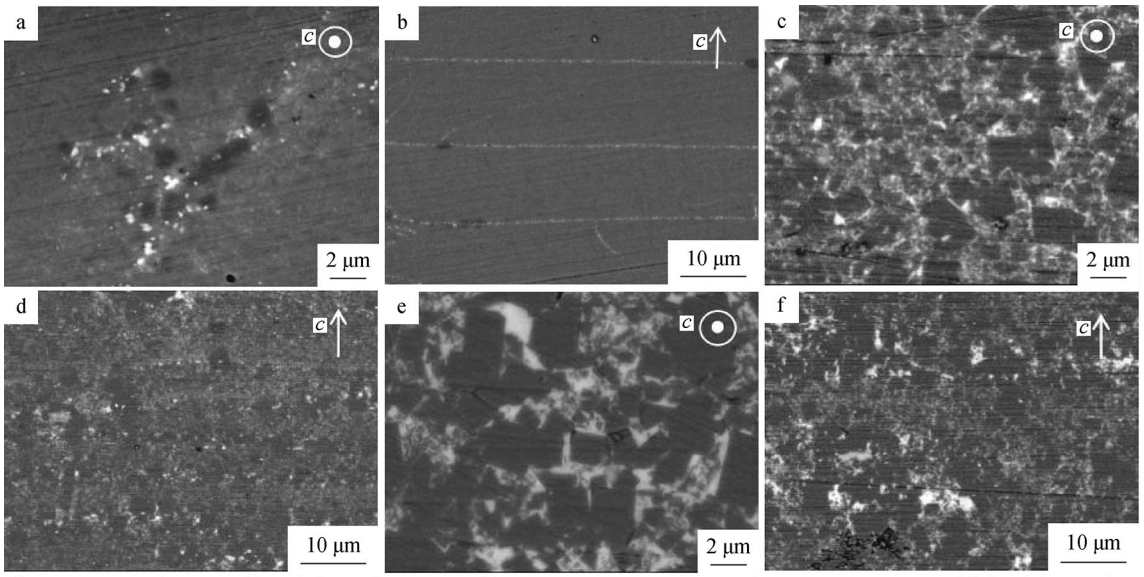

Fig. 4 BSE-SEM images of hot-deformed magnets with **a**, **b** 0 wt%, **c**, **d** 4 wt% and **e**, **f** 5 wt% $Pr_{85}Cu_{15}$ addition (observation plane being **a**, **c**, **e** perpendicular to *c*-axis and **b**, **d**, **f** parallel to *c*-axis)

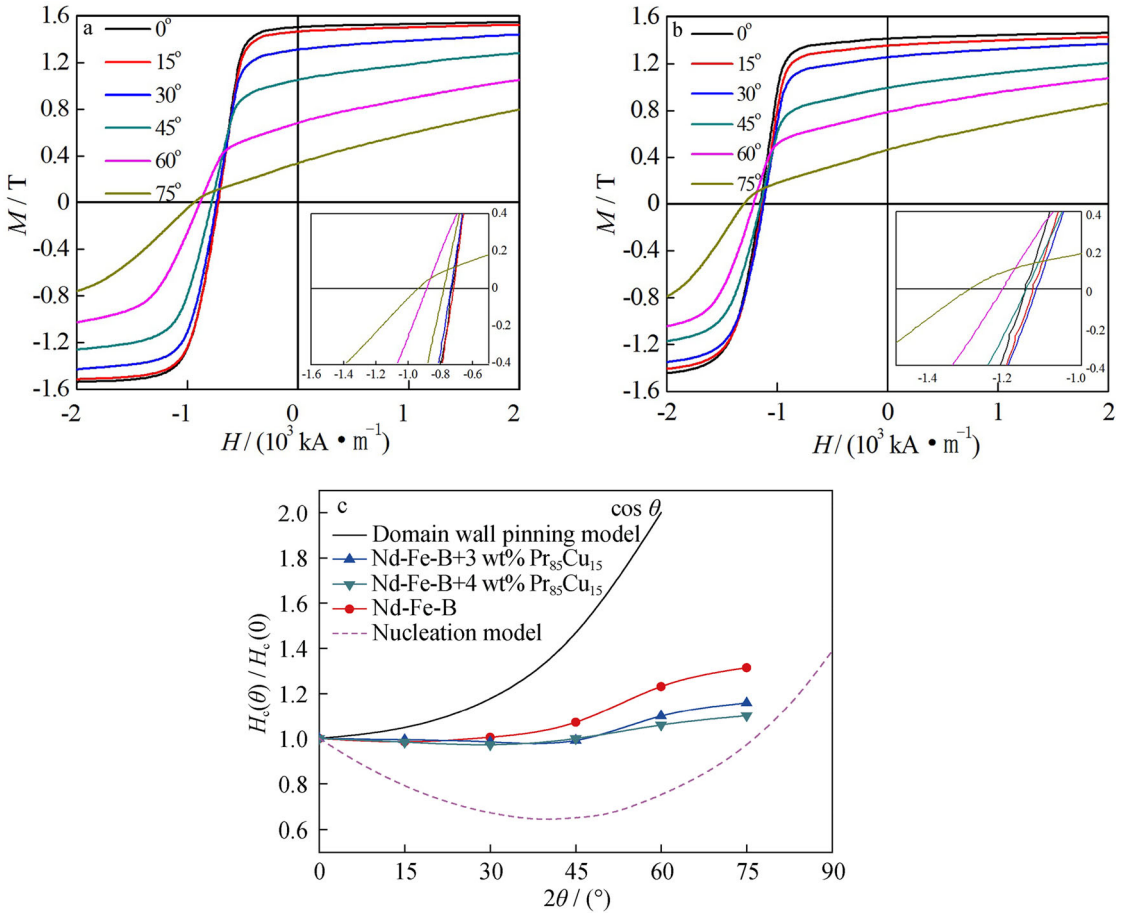

Fig. 5 Angular dependence of **a** Pr–Cu-free, **b** 3 wt% Pr–Cu addition half-hysteresis loop and partial enlarged detail, respectively, and **c** H_c for hot-deformed samples

is nucleation combined with domain wall pinning. During the changing process of H_c, the slope of the curves for the original hot-deformed sample is steeper than that of magnets with either 3 wt% or 4 wt% $Pr_{85}Cu_{15}$ addition, indicating that the domain wall pinning effect is weakened after adding $Pr_{85}Cu_{15}$ alloy.

Figure 6 presents the initial magnetization curves of the hot-deformed magnets with various $Pr_{85}Cu_{15}$ alloy additions. The magnetic susceptibility of the original sample is smaller than magnets with alloy addition when the external applied field is less than about 557.2 kA·m^{-1}, as shown in Fig. 6. And the magnetic susceptibility of the magnet with 4 wt% Pr–Cu alloy addition is bigger than that of the magnet with 3 wt% Pr–Cu alloy addition. The result indicates that the nucleation mechanism is enhanced with Pr–Cu alloy addition [30], which coincides well with the angular dependence of coercivity sloop.

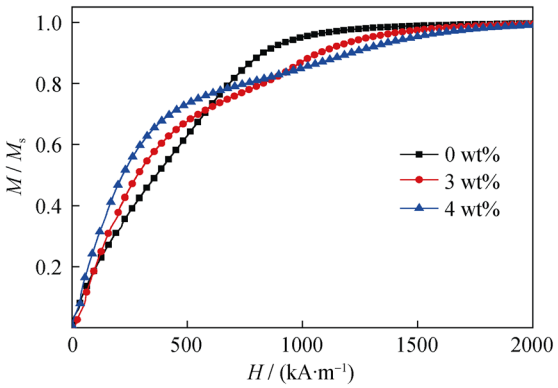

Fig. 6 Initial magnetization curves of hot-deformed magnets with various $Pr_{85}Cu_{15}$ alloy additions

4 Conclusion

A small amount of $Pr_{85}Cu_{15}$ alloy addition improves the coercivity of the hot-deformation Nd–Fe–B magnets obviously. The coercivity of the hot-deformation Nd–Fe–B magnets increases firstly and then decreases when $Pr_{85}Cu_{15}$

addition changes from 0 wt% to 5 wt%, and it exhibits the highest value when the addition is 4 wt%. SEM results show that a suitable Pr–Cu alloy addition leads to more RE phase around the main phase and uniform distribution that weaken the long-range magnetostatic interaction of neighboring grains and then enhance the coercivity. The magnetic properties of the magnet with 4.0% $Pr_{85}Cu_{15}$ addition are $B_r = 1.3$ T, $H_{cj} = 1271$ kA·m^{-1}, and $(BH)_{max} = 330.0$ kJ·m^{-3}. The coercivity with 4.0% $Pr_{85}Cu_{15}$ addition enhances by 75.69% compared to that of the original magnet (723 kA·m^{-1}). The angular dependence of coercivity and initial magnetization curves indicate that the coercivity mechanism of the hot-deformation Nd–Fe–B magnet is nucleation combined with domain wall pinning. The domain wall pinning mechanism is weakened, and nucleation is enhanced after Pr–Cu addition.

Acknowledgements This work was financially supported by the National Natural Science Foundation of China (No. 51331003) and the Major State Basis Research Development Program of China (No. 2014CB643701).

References

[1] Li AH, Zhao R, Lai B, Wang HJ, Zhu MG, Li W. Hot deformation in nanocrystalline Nd–Fe–B backward extruded rings. Chin Phys B. 2011;20(10):107503.
[2] Wang XC, Zhu MG, Li W, Li YF, Lai B, Du A. The microstructure and magnetic properties of anisotropic hot deformed magnet of the different magnetic particle size. Rare Met. 2015;34(4):255.
[3] Song J, Yue M, Zuo JH, Zhang ZR, Liu WQ, Zhang DT, Zhang JX, Guo ZH, Li W. Structure and magnetic properties of bulk nanocrystalline Nd–Fe–B permanent magnets prepared by hot pressing and hot deformation. J Rare Earth. 2013;31(7):674.
[4] Liu J, Sepehri-Amin H, Ohkubo T, Hioki K, Hattori A, Schrefl T, Hono K. Effect of Nd content on the microstructure and coercivity of hot-deformed Nd–Fe–B magnets. Acta Mater. 2013;61(14):5387.
[5] Lee RW. Hot-pressed neodymium–iron–boron magnets. Appl Phys Lett. 1985;49(8):790.
[6] Mishra RK, Chu TY, Rabenberg LK. The development of the microstructure of die-upset Nd–Fe–B magnets. J Magn Magn Mater. 1990;84(1–2):88.
[7] Grünberger W, Hinz D, Kirchner A, Müller KH, Schultz L. Hot deformation of nanocrystalline Nd–Fe–B alloy. J Alloy Compd. 1997;257(1):293.
[8] Lee RW, Brewer EG, Schaffel NA. Processing of neodymium–iron–boronmelt–spunribbons to fully dense magnets. IEEE Trans Magn. 1985;21(5):1958.
[9] Mishra RK, Lee RW. Microstructure, domain walls, and magnetization reversal in hot-pressed Nd–Fe–B magnets. Appl Phys Lett. 1986;48(11):733.
[10] Tenaud P, Chamberod A, Vanoni F. Texture in Nd–Fe–B magnets analysed on the basis of the determination of $Nd_2Fe_{14}B$ single crystals easy growth axis. Solid State Commun. 1987;63(4):303.
[11] Leonowicz M, Davies HA. Effect of Nd content on induced anisotropy in hot deformed Fe–Nd–B magnets. Mater Lett. 1994;19(5–6):275.
[12] Lai B, Wang HJ, Zhu MG, Li W. Simulation of die-upsetting process of hot-deformed magnets. J Korean Phys Soc. 2013;63(3):320.
[13] Li L, Luzzi DE, Graham CD. High-resolution electron microscope study of the grain boundary phase in rapidly quenched Nd–Fe–B permanent magnet alloy. J Matter Eng Perform. 1992;1(2):205.
[14] Croat JJ, Herbst JF, Lee RW, Pinkerton FE. High-energy product Nd–Fe–B permanent magnets. Appl Phys Lett. 1984;44(1):148.
[15] Croat JJ, Herbst JF, Lee RW, Pinkerton FE. Pr–Fe and Nd–Fe-based materials: a new class of high-performance permanent magnets (invited). J Appl Phys. 1984;55(6):2078.
[16] Thielsch J, Stopfel H, Wolff U, Neu V, Woodcock TG, Güth K, Schultz L, Gutfleisch O. In situ magnetic force microscope studies of magnetization reversal of interaction domains in hot deformed Nd–Fe–B magnets. J Appl Phys. 2012;111(10):103901.
[17] Liu J, Sepehri-Amin H, Ohkubo T, Hioki K, Hattori A, Schrefl T, Hono H. Grain size dependence of coercivity of hot-deformed Nd–Fe–B anisotropic magnets. Acta Mater. 2015;82:336.
[18] Sepehri-Amin H, Liu J, Ohkubo T, Hioki K, Hattori A, Hono K. Enhancement of coercivity of hot-deformed Nd–Fe–B anisotropic magnet by low-temperature grain boundary diffusion of $Nd_{60}Dy_{20}Cu_{20}$ eutectic alloy. Scripta Mater. 2013;69:647.
[19] Sepehri-Amin H, Ohkubo T, Nagashima S, Yano M, Shoji T, Kato A, Schrefl T, Hono K. High-coercivity ultrafine-grained anisotropic Nd–Fe–B magnets processed by hot deformation and the Nd–Cu grain boundary diffusion process. Acta Mater. 2013;61(17):6622.
[20] Liu LH, Sepehri-Amin H, Ohkubo T, Yano M, Kato A, Shoji T, Hono K. Coercivity enhancement of hot-deformed Nd–Fe–B magnets by the eutectic grain boundary diffusion process. J Alloy Compd. 2016;666:432.
[21] Ghandehari MH. Reactivity of Dy_2O_3 and Tb_4O_7 with $Nd_{15}Fe_{77}B_8$ powder and the coercivity of the sintered magnets. Appl Phys Lett. 1986;48(8):548.
[22] DeGroot CH, Buschow KHJ, de Boer FR, deKort K. Two powder $Nd_2Fe_{14}B$ magnets with DyGa addition. J Appl Phys. 1988;83(1):388.
[23] Sawatzki S. Dirba I, wendrock H, Schultz L, Gutfleisch O. Diffusion processes in hot-deformed Nd–Fe–B magnets with DyF_3 additions. J Magn Magn Mater. 2014;358–359(5):163.
[24] Watanabe N, Itakura M, Nishida M. Microstructure of high coercivity Nd–Fe–Co–Ga–B hot-deformed magnet improved by the Dy diffusion treatment. J Alloy Compd. 2013;557(6):1.
[25] Tang X, Chen RJ, Yin WZ, Lin M, Lee D, Yan AR. Mechanism analysis of coercivity enhancement of hot deformed Nd–Fe–B Magnets by DyF_3 diffusion. IEEE Trans Magn. 2013;49(7):3237.
[26] Du X, Jing Z, Han R, Guo ZH, Zhu MG, Li W. Microstructure and magnetic properties of high coercivity die-upset Nd–Fe–B magnets by Nd–Cu alloy addition. IEEE Trans Magn. 2015;51(11):2015003.
[27] Lai B, Li YF, Wang HJ, Li AH, Zhu MG, Li W. Quasi-periodic layer structure of die-upset NdFeB magnets. J Rare Earth. 2013;31(7):679.
[28] Lee Yuan T, Huang HL. Remodified Kondorsky function and asymmetric wall structure. J Appl Phys. 1993;74(1):495.
[29] Kronmüller H, Durst KD, Martinek G. J Magn Magn Mater. 1987;69:149.
[30] Kaplesh K. RE-TM5 and RE2-TM17 permanent magnets development. J Appl Phys. 1988;63(6):13.